Available online at www.sciencedirect.com
ScienceDirect
Journal of Solid State Chemistry 180 (2007) 1218–1223
JOURNAL OF SOLID STATE CHEMISTRY
www.elsevier.com/locate/jssc

Formation of α-Mn_2O_3 nanorods via a hydrothermal-assisted cleavage-decomposition mechanism

Youcun Chen[a], Yuanguang Zhang[a,b,*], Qi-Zhi Yao[b], Gen-Tao Zhou[c], Shengquan Fu[b], Hai Fan[b]

[a]*Provincial Key Laboratory of Functional Coordination Compounds and Department of Chemistry, Anqing Normal College, Anqing 246011, PR China*
[b]*Department of Chemistry, University of Science and Technology of China, Hefei 230026, PR China*
[c]*School of Earth and Space of Sciences, University of Science and Technology of China, Hefei 230026, PR China*

Received 26 October 2006; received in revised form 4 January 2007; accepted 7 January 2007
Available online 26 January 2007

Abstract

A hydrothermal cleavage-decomposition mechanism was used to synthesize single-crystal α-Mn_2O_3 nanorods at 160 °C for 16 h using $KMnO_4$ as manganese source and CTAB as reducing regent. The as-synthesized products were characterized by powder X-ray diffraction, transmission electron microscopy, high-resolution transmission electron microscopy and infrared spectrum. The results indicate that the reaction temperature is a crucial factor for the formation of α-Mn_2O_3 nanorods. These nanorods exhibit single-crystal nature, and have an average diameter of 36 nm and lengths of up to 1 μm. Based on our experimental results, a hydrothermal cleavage-decomposition mechanism has been proposed on the formation of α-Mn_2O_3 nanorods.

Keywords: Manganese oxides; Hydrothermal synthesis; Nanorod; Mechanism

1. Introduction

Manganese oxide materials are of considerable importance in technological applications including catalysis and rechargeable batteries, due to their outstanding structural flexibility combined with novel chemical and physical properties [1]. Polymorphs of Mn_2O_3 have been proposed as cheap, environmental-friendly catalysts for carbon monoxide [2] and organic pollutants [3–5] oxidation, and nitrogen oxide decomposition [6–8]. Intercalated Mn_2O_3 could improve greatly the stability of a nanocrystalline TiO_2 electrode during water splitting reactions under illumination of light, and could enhance the rate of oxygen evolution instead of H_2O_2 formation due to its catalytic effect [9]. Mn_2O_3 was also an important substrate for Li–Mn–O oxide cathode materials [10]. Many reports have been focused on the approaches to synthesize Mn_2O_3 materials. Tetragonal γ-Mn_2O_3 structure have recently been prepared by several methods, such as chemical oxidation of Mn^{2+} with H_2O_2 [11,12], reduction of $KMnO_4$ with hydrazine [13], ethanol-thermal reduction of MnO_2 [14], and γ-ray radiation of $KMnO_4$ solution [15]. α-Mn_2O_3 particles were usually prepared by heating MnO_2 or $MnCO_3$ in air at temperatures of 600–800 °C [16]. Sphere- or cube-like α- Mn_2O_3 was obtained at 550 °C through the decomposition of the $MnCO_3$ precursors synthesized via a hydrothermal reduction route [17]. Nanofiberous α-Mn_2O_3 was prepared by calcination of preformed γ-MnO_2 nanowires at the temperature above 600 °C [18]. Single-crystalline α-Mn_2O_3 nanorods were also synthesized at 250 °C for 24 h by ammonia-hydrothermal treatment of MnO_2 [19] and at 600–800 °C for 8–16 h in air by heat treatment of γ-MnOOH [20], respectively. In addition, it had been reported that ammonium salts were used as reducing agents in the synthesis of MnO_2 and MnOOH [21], and $KMnO_4$ can interact with CTAB in the solutions [22]. Here, we report a low-temperature

*Corresponding author. Provincial Key Laboratory of Functional Coordination Compounds, Anqing Normal College, Anqing 246011, PR China. Fax: +86 556 550 0090.
E-mail address: ygz@mail.ustc.edu.cn (Y. Zhang).

0022-4596/$ - see front matter © 2007 Elsevier Inc. All rights reserved.
doi:10.1016/j.jssc.2007.01.017

hydrothermal-assisted process to prepare single-crystal α-Mn_2O_3 nanorods, using $KMnO_4$ as manganese source and CTAB as reducing regent without post-calcinations treatment, and a hydrothermal-assisted cleavage-decomposition growth mechanism was revealed.

2. Experimental procedure

All the reagents were analytical reagent grade, and were used without further purification. In a typical process, 0.002 mol of $KMnO_4$ and 0.003 mol of CTAB were put into distilled water at room temperature to form a brown solution, which was then transferred into a Teflon-lined stainless steel autoclave of 60 ml capacity, and filled with distilled water up to 80% of the total volume. The autoclave was sealed and maintained at 160 °C for 16 h. After that, the autoclave was allowed to cool to room temperature naturally. The resultant products were collected by filtration, washed several times with distilled water and absolute ethanol to remove impurities, and then dried under a vacuum at 50 °C for 3 h. In addition, according to the above procedure, some experiments were made in the absence of CTAB, no any products were obtained.

The X-ray powder diffraction (XRD) patterns were recorded on a Philips X'pert diffractometer using Cu$K\alpha$ radiation ($\lambda = 0.15418$ nm). Transmission electron microscopy (TEM) images were taken using a Hitachi Model H-800 microscope. The high-resolution transmission electron microscopy (HRTEM) images were taken using JEOL-2010F high-resolution transmission microscope operated at 200 kV. The infrared spectrum (IR) was recorded on a Bruker Vector-22 FT-IR spectrometer from 400 to 4000 cm^{-1} at room temperature on KBr mulls. The samples used for characterization were dispersed in absolute ethanol and were ultrasonicated before SEM and TEM observation.

3. Results and discussion

The XRD pattern of the product synthesized at 160 °C for 16 h was shown in Fig. 1. All of the reflections in this pattern can be readily indexed to a cubic phase [space group: $12_13(199)$] of α-Mn_2O_3 with the calculated lattice constants $a = 0.9417$ nm, which are in good agreement with the literature results (JCPDS No.76-0150). From this pattern, it can be seen that the product has a high crystallinity.

The IR spectrum of the product synthesized at 160 °C for 16 h is shown in Fig. 2. The peaks at about 3448 and 1632 cm^{-1} can be assigned to υ_{O-H} stretching vibration and bending vibration of water molecules adsorbed by the Mn_2O_3 products, respectively [23]. The peaks around 665and 586 were attributed to υ_{Mn-O} stretching vibration of Mn_2O_3, 528 cm^{-1} were attributed to υ_{Mn-O} bending vibration of Mn_2O_3 [24]. This pattern further confirmed

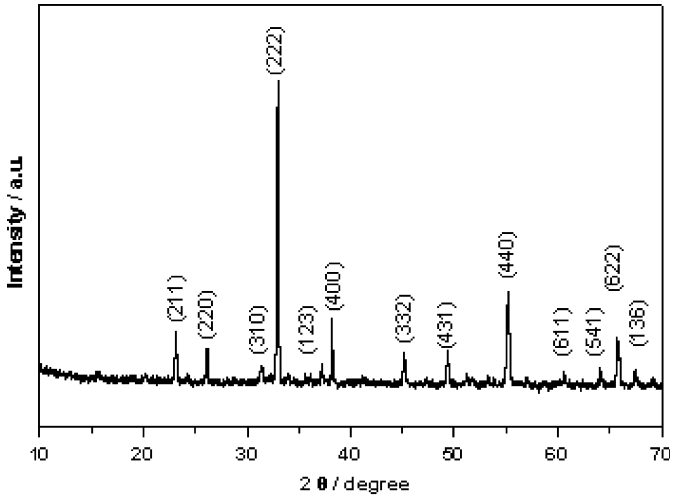

Fig. 1. XRD pattern of the product synthesized at 160 °C for 16 h.

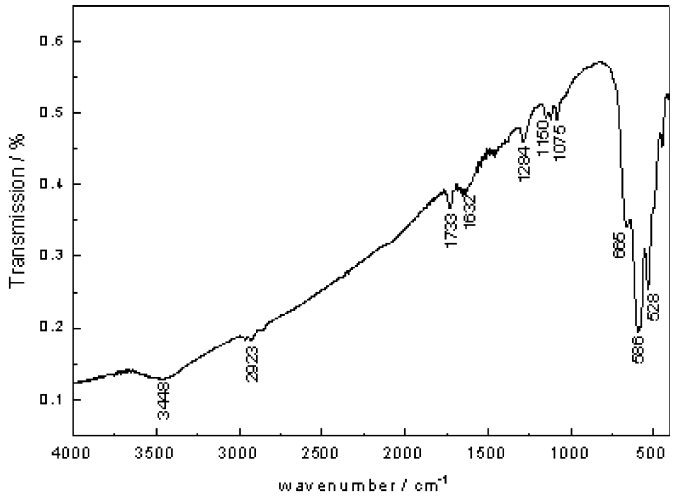

Fig. 2. IR spectrum of the product synthesized at 160 °C for 16 h.

that the products synthesized at 160 °C for 16 h are Mn_2O_3 phase, which is in agreement with analysis result of XRD.

The structure of the Mn_2O_3 product obtained at 160 °C for 16 h was examined by TEM and HRTEM techniques. It can be seen from Fig. 3a that the Mn_2O_3 product displays rod-like morphology. These nanorods have a mean diameter of ca. 36 nm and lengths of up to 1 μm. Fig. 3b is a single nanorod randomly selected from the Mn_2O_3 product. The inset in Fig. 3b is the corresponding selected area electron diffraction (SAED) pattern. It is observed that the SAED pattern consists of many spots. All spots are identified as the diffractions from cubic Mn_2O_3, which reveals the single-crystalline nature of Mn_2O_3 nanorods. The HRTEM image (Fig. 3c) shows that the lattice fringes of the nanorod shown in Fig. 3b are structurally uniform, and the interplannar spacings are about 0.27 and 0.38 nm, which correspond to the (222) and (211) planes of Mn_2O_3, respectively. It further confirms the single-crystalline nature of the Mn_2O_3 nanorods. Fig. 3c

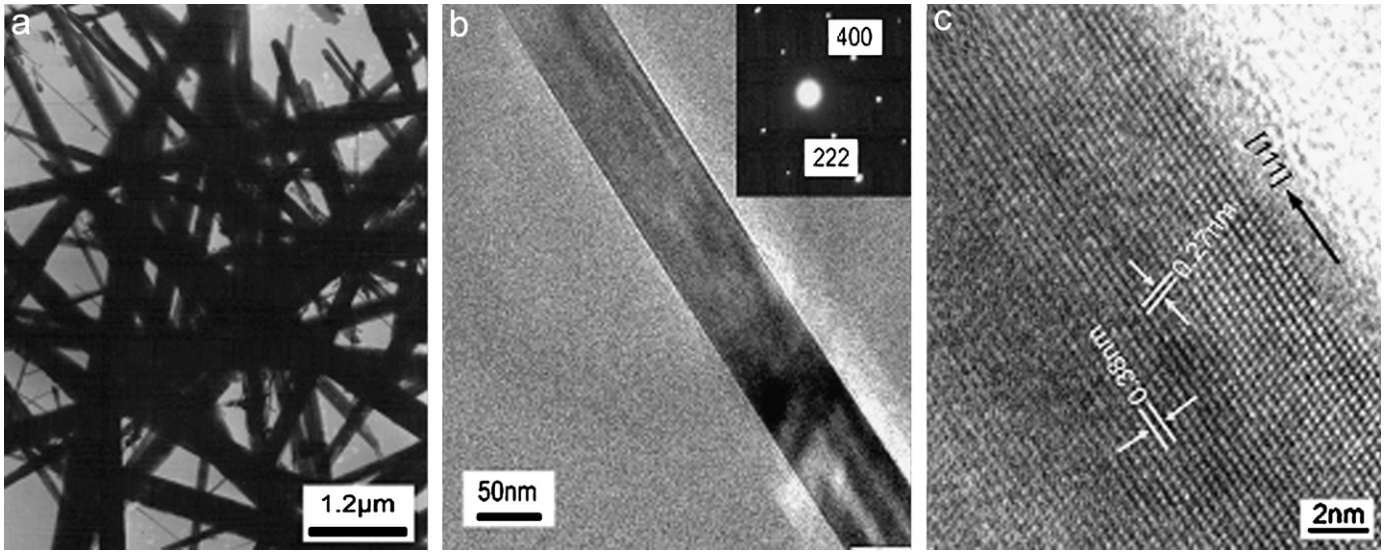

Fig. 3. (a) TEM image of the Mn_2O_3 product obtained at 160 °C for 16 h; (b) TEM image and SAED pattern (inset) of a single nanorod randomly selected from the Mn_2O_3 product; (c) HRTEM image of the nanorod shown in Fig. 3b.

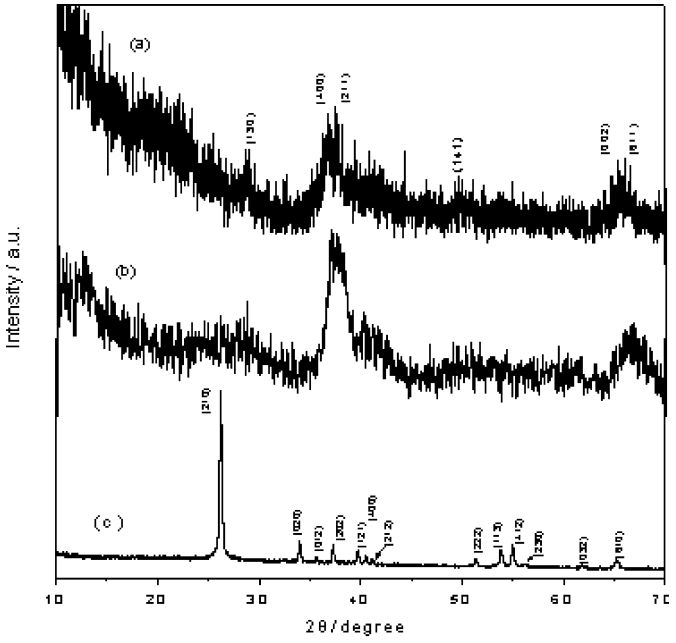

Fig. 4. XRD patterns of the products synthesized at different temperatures for 16 h: (a) 100 °C; (b) 130 °C; (b) 190 °C.

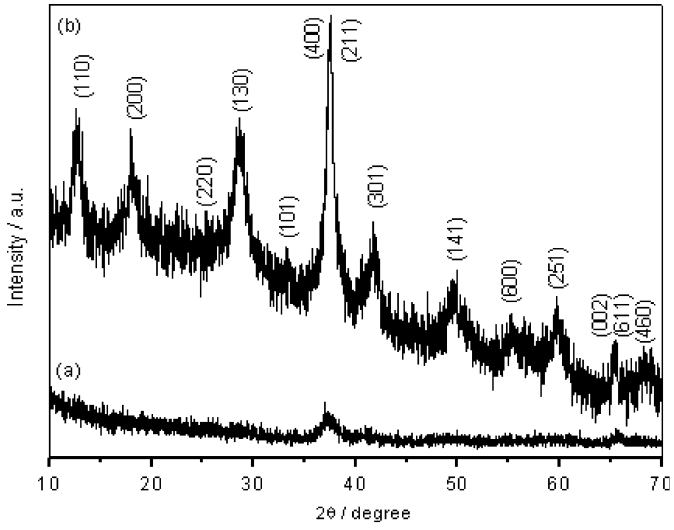

Fig. 5. XRD patterns of the products synthesized at different reaction time: (a) 2 h; (b) 10 h.

also shows that these nanorods grow preferentially along the [111] direction.

In order to insight into the formation mechanism of Mn_2O_3 nanorods, some comparative experiments were carried out at 100 and 190 °C keeping the otherwise experimental conditions unchanged. It was found that the product synthesized at 100 °C or 130 °C for 16 h, could be indexed to a tetragonal phase of $K_{1.33}Mn_8O_{16}$ (Figs. 4a and 4b), which agrees well with literature values (JCPDS No. 77-1796). The product synthesized at 190 °C for 16 h, can be indexed to a monoclinic phase of MnOOH (Fig. 4c), which agrees well with literature values (JCPDS No. 74-1632). XRD results indicate that the reaction temperature plays crucial role in the formation of Mn_2O_3 nanorods. On the other hand, keeping the reaction temperature at 160 °C, some experiments with different reaction times from 2, 4, 8 to 10 h reveal that the products synthesized from 2 h to 10 h are tetragonal single-phase of $K_{1.33}Mn_8O_{16}$, which was confirmed by XRD results (Fig. 5). TEM results showed that the product synthesized for 2 h was composed of cone-like particles, rod-like particles, and irregular particles, as shown in Fig. 6a. With the reaction time of 4 h, as shown in Figs. 6b and 6c, the product mainly consisted of cone-like particles, and some cones were assembled into one-dimensional cone-structures. The SAED pattern for the single cone shown in Fig. 6d displays many spots, which can be indexed

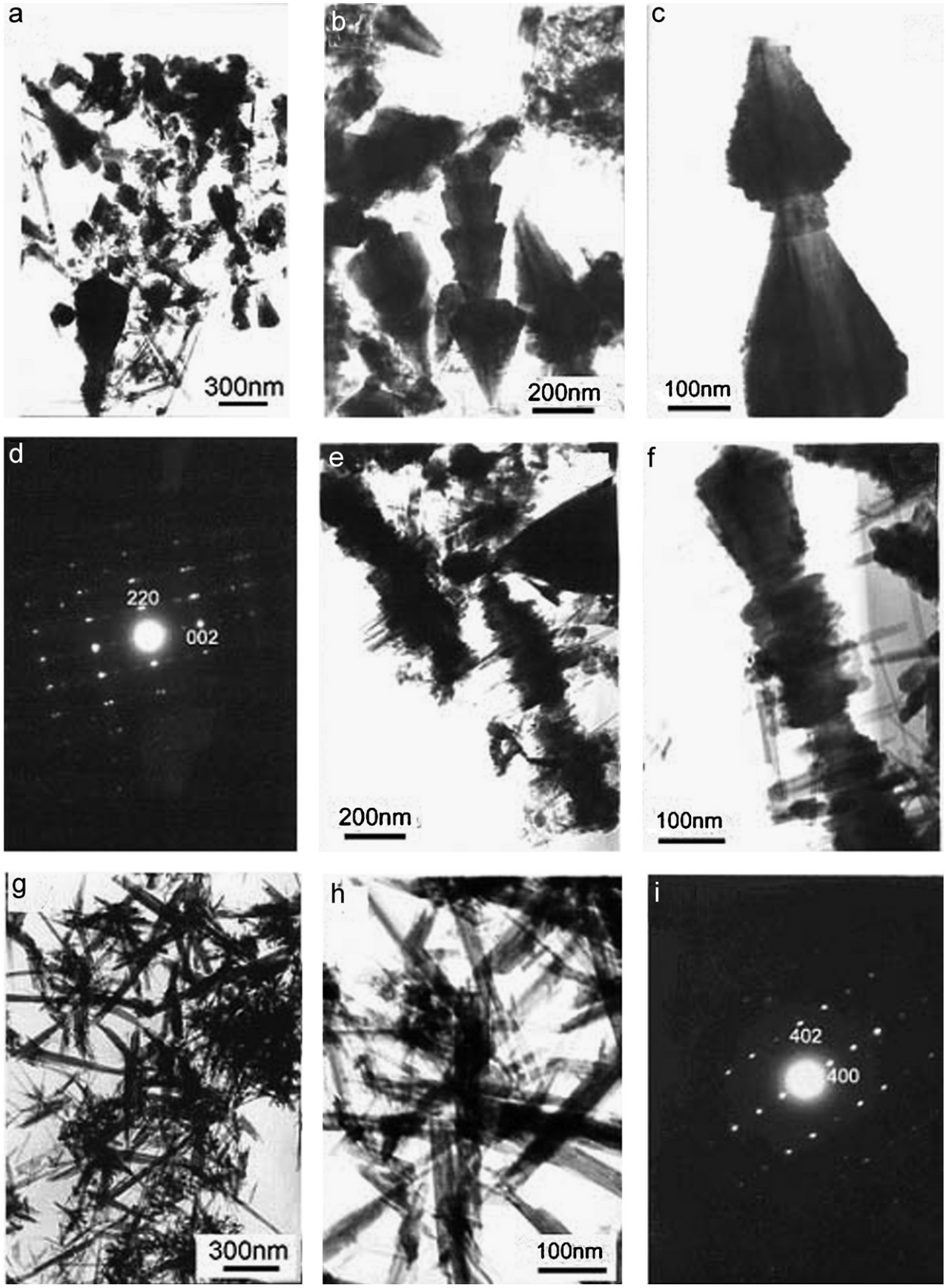

Fig. 6. TEM images and SAED patterns of the products obtained at 160 °C for different reaction times: (a) 2 h; (b), (c) and (d) 4 h; (e) and (f) 8 h; (g), (h) and (i) 10 h.

tetragonal $K_{1.33}Mn_8O_{16}$ phase. It indicates the single-crystal nature of the cone structure. With prolonging reaction time to 8 h, a small amount of rod-like structure and the cleaved cone-like structure coexist, as shown in Figs. 6e and f, and these images also indicate that the cleavage direction of the cones is perpendicular to the cone axes. With the reaction time of 10 h, as shown in Figs. 6g and 6h, the product was mainly composed of nanorods. The SAED pattern shown in Fig. 6i has many spots, which can be indexed tetragonal $K_{1.33}Mn_8O_{16}$ phase. It shows the single-crystal nature of $K_{1.33}Mn_8O_{16}$ nanorods. The above processes are shown in Fig. 7.

Based on the above experimental results and $K_{1.33}Mn_8O_{16}$ crystal structure, it could be deduced that the α-Mn_2O_3 nanorods were formed by a cleavage-decomposition process of the intermediates. In our experiments, an intermediate $K_{1.33}Mn_8O_{16}$ will first form, its morphologies evolve from irregular particles to 1D cone structures, finally formed rod-like structures by the cleavage of cone structures. The rod-like structures of $K_{1.33}Mn_8O_{16}$ were gradually decomposed to form α-Mn_2O_3 nanorods. This conclusion was accordance with the literature reports. Strobel et al. [25] reported that $K_{1.33}Mn_8O_{16}$ powders could be prepared by aqueous chemistry, and decomposed to Mn_2O_3 in the range of 460–610 °C in air, and Faulring et al. [26] reported that

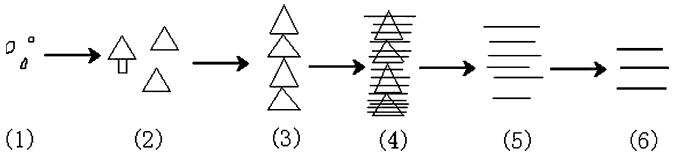

Fig. 7. The formation processes of α-Mn_2O_3 rod-like structures. (1) $K_{1.33}Mn_8O_{16}$ irregular particles; (2) $K_{1.33}Mn_8O_{16}$ core structures; (3) $K_{1.33}Mn_8O_{16}$1D cone structures; (4) $K_{1.33}Mn_8O_{16}$ cleavage perpendicular to cone axes; (5) $K_{1.33}Mn_8O_{16}$ rod-like structures; (6) α-Mn_2O_3 rod-like structures.

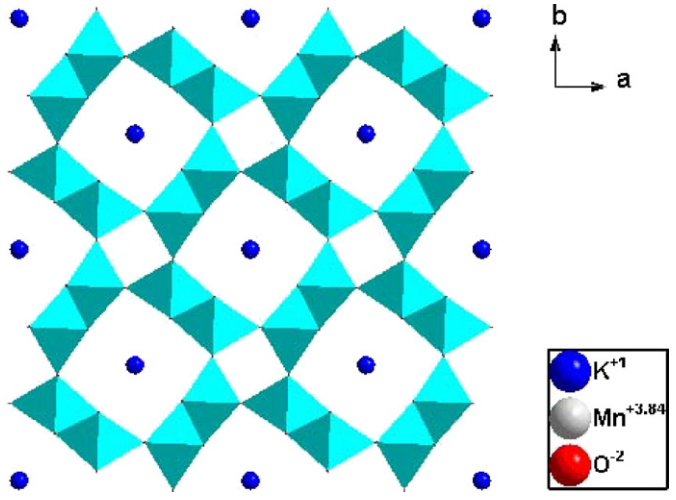

Fig. 8. Structure of $K_{1.33}Mn_8O_{16}$ projected along (001) planes ($2 \times 2 \times 2$ lattices).

heating $K_{1.33}Mn_8O_{16}$ columnar crystal at air resulted in the produce of Mn_2O_3 with high oriented. On the other hand, form the $K_{1.33}Mn_8O_{16}$ crystal structure as shown in Fig. 8, manganese ions are in MnO_6-octahedra, which are linked to form double octahedral zigzag chains along the *c*-axis by edge-sharing. These chains share their corners with each other to form approximately square tunnels parallel to the *c*-axis. The K^+ cations are located within the tunnels, being surrounded by eight oxygen ions. The crystal symmetry is mostly tetragonal (space group; $I4/m$). This Hollandite-type $K_{1.33}Mn_8O_{16}$ structure is favorable to the formation of α-Mn_2O_3 nanorods. Post and Yamamoto had reported that Mn^{3+} is the reduced form of Mn for Hollandite-type structure, because the mean Mn–O bond lengths in MnO_6 octahedron calculated from the refinement suggest that Mn^{3+} is more easily accommodated in the structures than the larger Mn^{2+} [27].

4. Conclusions

Single-crystal α-Mn_2O_3 nanorods with an average diameter of 60 nm and length of up to 1 μm were hydrothermally synthesized at 160 °C for 16 h in the presence of CTAB. The reaction temperature played very important roles in the formation of α-Mn_2O_3 nanorods. This hydrothermal cleavage-decomposition mechanism may be extended to synthesize 1D structures of other manganese oxides.

Acknowledgments

This work was supported by the National Natural Science Foundation of China (20371002) and Education office Key Project of Anhui Province (2006kj042A).

Reference

[1] M.M. Thackeray, Prog. Solid State Chem. 25 (1997) 1.
[2] S. Imamura, M. Shono, N. Okamoto, A. Hamada, S. Ishida, Appl. Catal. A 142 (1996) 279.
[3] H.M. Zhang, Y. Teraoka, N. Yamazoe, Catal. Today 6 (1989) 155.
[4] M. Baldi, V. Sanchez Escribano, J.M. Gallardo Amores, F. Milella, G. Busca, Appl. Catal. B 17 (1998) L175.
[5] L.M. Gand, S.A. Korili, A. Gil, Stud. Surf. Sci. Catal. 143 (2002) 527.
[6] T. Yamashita, A. Vannice, J. Catal. 161 (1996) 254.
[7] T. Yamashita, A. Vannice, J. Catal. 163 (1996) 158.
[8] A. Vannice, T. Yamashita, Appl. Catal. B 13 (1997) 141.
[9] S.U.M. Khan, J. Akikusa, J. Electrochem. Soc. 145 (1998) 89.
[10] T. Nakamura, A. Kajiyama, Solid State Ionics 124 (1999) 45.
[11] S. Zhang, Z. Chen, S. Tan, J. Wang, S. Jin, Nanostruct. Mater. 8 (1997) 719.
[12] Z. Chen, S. Zhang, S. Tan, F. Li, J. Wang, S. Jin, Y. Zhang, J. Cryst. Growth 180 (1997) 280.
[13] Z. Gui, R. Fan, X.H. Chen, Y.C. Wu, Inorg. Chem. Commun. 4 (2001) 294.
[14] W.L. He, Y.C. Zhang, X.X. Zhang, H. Wang, H. Yan, J. Cryst. Growth 252 (2003) 285.
[15] Y. Liu, Y. Qian, Y. Zhang, M. Zhang, Z. Chen, L. Yang, C. Wang, Z. Chen, Mater. Lett. 28 (1996) 357.
[16] M. Tabuchi, K. Ado, J. Electrochem. Soc. 145 (1998) L49.

[17] S.J. Lei, K.B. Tang, Z. Fang, Q.C. Liu, H.G. Zheng, Mater. Lett. 60 (2006) 53.
[18] Z.Y. Yuan, Z. Zhang, G.H. Du, T.Z. Ren, B.L. Su, Chem. Phys. Lett. 378 (2003) 349.
[19] Z.Y. Yuan, T.Z. Ren, G.H. Du, B.L. Su, Chem. Phys. Lett. 389 (2004) 83.
[20] Z.H. Yang, Y.C. Zhang, W.X. Zhang, X. Wang, Y.T. Qian, X.G. Wen, S.H. Yang, J. Solid State Chem. 179 (2006) 679.
[21] Y.G. Zhang, Y. Liu, F. Guo, Y.H. Hu, X.Z. Liu, Y.T. Qian, Solid State Commun. 134 (2005) 523.
[22] W.L. Wang, H. Jiang, Z.Q. Liu, X.M. Liu, J. Mater. Chem. 15 (2005) 1002.
[23] Y. Liu, W. Ren, L.Y. Zhang, X. Yao, Thin Solid Films 353 (1999) 124.
[24] B. Gillot, M. El Guendouzi, M. Laarj, Mater. Chem. Phys. 70 (2001) 54.
[25] P. Strobel, J. Vicat, D.T. Qui, J. Solid State Chem. 55 (1984) 67.
[26] G.M. Faulring, W.K. Zwicker, W.D. Forgeng, Am. Mineral 45 (1960) 946.
[27] Y. Muraoka, H. Chiba, T. Atou, M. Kikuchi, K. Hiraga, Y. Syono, J. Solid State Chem. 144 (1999) 136.